Available online at www.sciencedirect.com
SCIENCE DIRECT®
International Journal of Solids and Structures 43 (2006) 2–26
INTERNATIONAL JOURNAL OF SOLIDS and STRUCTURES
www.elsevier.com/locate/ijsolstr

Finite element modelling of rubber-like polymers based on chain statistics

M. Böl, S. Reese *

Department of Civil Engineering, Institute of Mechanics, Ruhr University Bochum, Universitätsstraße 150, D-44801 Bochum, Germany

Received 23 July 2004; received in revised form 8 June 2005
Available online 26 October 2005

Abstract

In this work finite element simulations are conducted based on the micro structure of polymers in order to transfer the information of the micro level to the macro level. The micro structure of polymers is characterized by chain-like macromolecules linked together at certain points. In this way an irregular three-dimensional network is formed. Many authors use the tool of statistical mechanics to describe the deformation behaviour of the entire network. Most of these concepts can be reformulated as traditional continuum mechanical formulations. They are, however, restricted to affine deformation, regular chain arrangements and purely elastic material behaviour. For this reason, in the present contribution, we propose a new finite element-based simulation method for polymer networks which enables us to include non-affinity and arbitrary chain configurations. It can be easily extended to include chain breakage and reconnection.

The polymer structure to be investigated, e.g. a rubber boot or a seal, is discretized by means of tetrahedral elements. To each edge of a tetrahedral element one truss element is attached which models the force–stretch behaviour of a bundle of polymer chains. Each of these tetrahedral unit cells represents the micro mechanical material behaviour in a certain point of the network. The proposed method provides the possibility to observe how changes at the microscopic level influence the macroscopic material behaviour. Such information is especially valuable for the polymer industry.

Keywords: Polymer network; Non-linear elasticity; Near-incompressibility; Tetrahedral elements; Selective reduced integration

1. Introduction

The microscopic structure of polymers consists of long, randomly oriented molecular chains which are linked together at certain points. In this way an arbitrary three-dimensional network is formed. In addition there exist intermolecular interactions between the particular atoms which have an important influence on the dilatational response of rubber-like material (see e.g. Gaylord, 1979; Ball et al., 1981; Gao and Weiner, 1991; Lodge, 1999).

* Corresponding author. Tel.: +49 (0)234 32 25883; fax: +49 (0)234 32 14488.
E-mail address: reese@nm.ruhr-uni-bochum.de (S. Reese).

0020-7683/$ - see front matter © 2005 Elsevier Ltd. All rights reserved.
doi:10.1016/j.ijsolstr.2005.06.086

Several authors have studied the micro mechanical behaviour by means of molecular-dynamics simulations. Complex techniques, as e.g. the Monte Carlo method or the bond fluctuation method, have been developed for this purpose (Wittkop et al., 1994; Hölzl et al., 1997; Lang et al., 2003). These approaches have in common that in the discretized model each chain or even chain link is represented separately. In this way for instance the vulcanization process can be modelled very realistically. However, such simulations require an extreme computational effort. Therefore they are usually carried out at the level of a representative volume element. It is improbable that the step to model complex structures, such as e.g. seals or bearings, can be made in the near future.

The numerical modelling can be noticeably simplified if the tools known from statistical mechanics are incorporated (see e.g. Kuhn, 1936; Wall, 1942; Flory and Rehner, 1943; James and Guth, 1943; Treloar, 1943). The latter models are based on the assumption that the bonds of the network are permanent (static network theory). Furthermore the following assumptions have been established:

(i) All chains of the network have the same length nl in the totally extended state (n, number of chain links and l, average length of a chain link).
(ii) The distribution of the end-to-end distances r_0 of the chains is calculated by means of Gaussian statistics.
(iii) The deformation of the material is affine.
(iv) There is no change in volume.

Based on these assumptions Treloar (1943) derived the well-known "Neo-Hookean" free energy function (per reference volume) $W = (\mu/2)(\lambda_1^2 + \lambda_2^2 + \lambda_3^2 - 3)$ where λ_i $(i = 1, 2, 3)$ represent the principal stretches and $\mu = Nk\Theta$ denotes the rubber shear modulus (N, number of chains per reference volume; k, Boltzmann's constant; Θ, absolute temperature). This network model is only suitable for moderate strains and therefore does not correlate well with experiments for large strains. This problem has been overcome by newer models, e.g. the ones of Arruda and Boyce (1993), Wu and van der Giessen (1993), Anand (1996) and Bischoff et al. (2002). The mentioned concepts are based on the Langevin statistics which has been originally suggested by Kuhn and Grün (1942). However, also the more recent network theories work with the assumptions (i), (iii) and (iv).

Alternatively, to overcome the deficiency of the Neo-Hooke model, rubber-like materials can be described by purely continuum-based models. Among the most popular ones of this kind are the concepts of Mooney (1940), Rivlin (1948) and Ogden (1972). The best agreement with experiments is displayed by the Ogden model. The disadvantage of the latter approaches with respect to the models based on chain statistics lies in the fact that the material parameters are not physically motivated. As such they can only be found by means of experiments. This fitting procedure can be very elaborate if the number of parameters is large. Further there is usually not only one set of material parameters which yields a good correlation with the experimental data (non-uniqueness).

This is the reason why in the present contribution a micro mechanically based approach is preferred. In comparison to earlier works we aim to avoid the assumptions (i)–(iv). The transfer of the known micro mechanical material behaviour to the macroscopic level by means of the finite element method is crucial to the work.

The proposed approach is based on the idea of representing the polymer network by means of an assembly of non-linear truss elements. Each truss element models the force–stretch behaviour of a certain group of chains. The truss elements are configured in such a way that six of them form a cell of tetrahedral shape. These tetrahedral elements serve to model the hydrostatic pressure built up in the network. Using a random assembling procedure we are in the position to model arbitrary geometries. Another advantage of this concept is the possibility to treat chain breakage and reconnection, i.e. inelasticity. Alternative finite element-based concepts have been suggested by André et al. (2001) and Lulei and Miehe (2001). Of further interest is also the work of Besdo and Ihlemann (2003) who propose the so-called theory of self-organizing linkage patterns to model typical rubber non-linearities such as hysteresis and stress softening.

The paper is structured as follows. In Section 2 the modelling of the force–stretch behaviour of a single polymer chain is discussed in detail. To obtain a realistic response of the full network, near-incompressibility has to be taken into account. This is achieved by the addition of another volumetric contribution in the center of each unit cell. In Section 3 we derive the corresponding finite element formulation. The transition from the

micro to the macro transition is discussed in Section 4. Section 5 gives a circumstantial survey of the numerical simulation. We examine in detail the influence of micro mechanical properties, such as e.g. the chain length and the chain configuration, on the macroscopic behaviour. The section closes with a study of convergence with respect to mesh refinement. In Section 6 the proposed concept is validated by means of a comparison with experimental results. The paper closes with a summary and an outlook to future work.

2. Material modelling

2.1. Statistical mechanics of the micro structure—the single chain

One fundamental material property of rubber-like material is its high elasticity which permits stretching of several hundred percent. The reason for this behaviour is the particular micro structure of rubber. It is characterized by a huge number of chain-like macromolecules which form a three-dimensional network. The material exhibits so-called statistical behaviour, i.e. the network configuration actually taken on by the material is the most probable one under the given circumstances.

The aim of this section is to describe the material behaviour of a single chain. This problem was e.g. tackled by Kuhn and Grün (1942). By means of the so-called Langevin function $\mathscr{L}(\beta) = \coth\beta - 1/\beta$ it is possible to derive an expression for the entropy of the single chain. Assuming further that the internal energy of the chain can be neglected the Helmholtz free energy is given by

$$W_{\text{chain}} = kn\Theta\left(\frac{\lambda_{\text{chain}}}{\sqrt{n}}\beta\gamma + \ln\frac{\beta}{\sinh\beta}\right) \tag{1}$$

In Eq. (1) the stretch of the single chain is described by $\lambda_{\text{chain}} = r/r_0$ where r describes the end-to-end distance of the loaded chain and the initial chain length is represented by

$$r_0 = l\sqrt{n}\sqrt{\frac{(1+\cos\vartheta)}{(1-\cos\vartheta)}}\sqrt{\frac{(1+\cos\varphi)}{(1-\cos\varphi)}} := l\sqrt{n}\gamma \tag{2}$$

The variable φ describes the rotation angle. The bond angle $\vartheta = 180° - \delta$ can be calculated by the use of the valence angle δ (see also Fig. 10). For a discussion of the influence of r_0 on the macroscopic behaviour, see Section 5.3. The factor β can be expressed in form of the series expansion (see e.g. Kuhn and Grün, 1942)

$$\begin{aligned}\beta &= \mathscr{L}^{-1}\left(\frac{\lambda_{\text{chain}}}{\sqrt{n}}\gamma\right)\\ &\approx 3\frac{\lambda_{\text{chain}}}{\sqrt{n}}\gamma + \frac{9}{5}\left(\frac{\lambda_{\text{chain}}}{\sqrt{n}}\gamma\right)^3 + \frac{297}{175}\left(\frac{\lambda_{\text{chain}}}{\sqrt{n}}\gamma\right)^5 + \frac{1539}{875}\left(\frac{\lambda_{\text{chain}}}{\sqrt{n}}\gamma\right)^7 + \frac{672}{359}\left(\frac{\lambda_{\text{chain}}}{\sqrt{n}}\gamma\right)^9\\ &\quad + \frac{10877}{5446}\left(\frac{\lambda_{\text{chain}}}{\sqrt{n}}\gamma\right)^{11} + \frac{3427}{1622}\left(\frac{\lambda_{\text{chain}}}{\sqrt{n}}\gamma\right)^{13} + \frac{13771}{6253}\left(\frac{\lambda_{\text{chain}}}{\sqrt{n}}\gamma\right)^{15} + \frac{3999}{1775}\left(\frac{\lambda_{\text{chain}}}{\sqrt{n}}\gamma\right)^{17}\\ &\quad + \frac{2249}{997}\left(\frac{\lambda_{\text{chain}}}{\sqrt{n}}\gamma\right)^{19}\end{aligned} \tag{3}$$

It is recognized in (3) that β depends on n, the number of approximation terms in the series expansion, here called TA, and on γ. Fig. 1 shows the influence of n and TA on the relation between the chain force

$$F_{\text{chain}} = \frac{\partial W_{\text{chain}}}{\partial r} = \frac{\partial W_{\text{chain}}}{\partial \lambda_{\text{chain}}}\frac{1}{r_0} + \frac{\partial W_{\text{chain}}}{\partial \beta}\frac{\partial \beta}{\partial \lambda_{\text{chain}}}\frac{1}{r_0} \tag{4}$$

and the stretch of the single chain λ_{chain}. An increase of n leads to a decrease of the chain stiffness, especially for higher stretches (see Fig. 1(a)). A similar tendency is observed if TA is decreased (see Fig. 1(b)). At the chain level we do not obtain a converged solution with increasing TA. This is certainly a surprising result which has not yet been documented in the literature (to our knowledge). However, it will be shown in Section 5.3 that convergence is obtained at the macro level (see Fig. 8(a)). Ten terms in the series expansion (TA = 10) are sufficient.

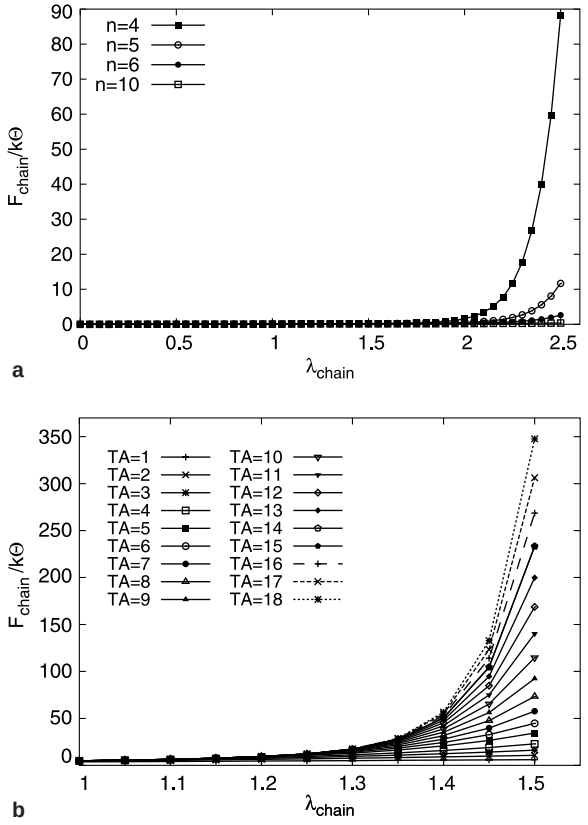

Fig. 1. Tensile behaviour of a single chain ($\gamma = 1$): (a) variation of n (TA = 10), (b) variation of TA ($n = 4$).

Fig. 2 depicts the influence on the force–stretch behaviour of the third parameter γ for a single chain. The valence angle is usually equal to 109.5° ($\vartheta = 70.5°$). The rotation angle (described by φ) varies between −120° and 120°. Accordingly γ lies in the interval $0.8165 < \gamma < \infty$, however typically around 1 ($\varphi = 109.5°$). In the present work the characteristic angles have been assumed to be constant for simplicity. Future investigations should be directed to include statistical distributions.

An increase of γ leads to stiffer force–stretch behaviour. It is easy to find an explanation for this observation if one compares the chain with one of the truss configurations shown in Fig. 3. The totally extended state (indicated by the index "ex") is reached at $\lambda_{ex} = r_{ex}/r_0 = nl/(nl\cos\vartheta) = 1/\cos\vartheta$. The value of λ_{ex} for configuration 2 is smaller than for configuration 1 ($\vartheta_2 < \vartheta_1$). Even if all trusses have the same stiffness and the

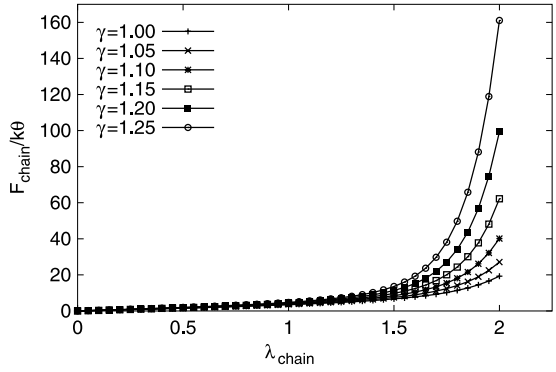

Fig. 2. Tensile behaviour of a single chain: variation of γ.

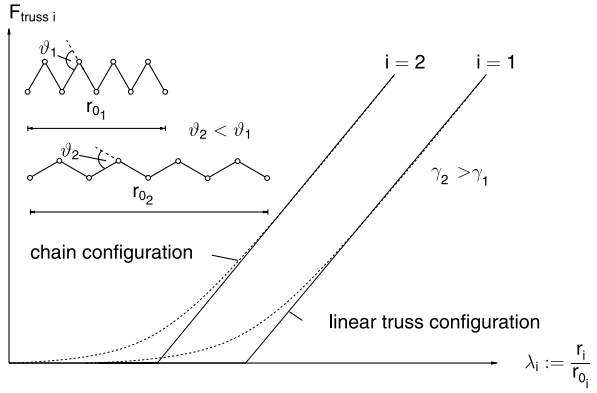

Fig. 3. Tensile behaviour of two linear trusses (solid lines) and two chain configurations (dashed lines): variation of γ (inset: two truss configurations).

force–displacement relation is linear, different curves are obtained. A similar effect is seen in Fig. 2 where, however, the slope of the curves is always positive and the increase of the force therefore more smoothly.

We also emphasize the well-known fact that the force is *not* zero for $\lambda_{\text{chain}} = 1$. It vanishes for $\lambda_{\text{chain}} = 0$, i.e. $r = 0$ (see Figs. 1 and 2). This result arises from applying statistical mechanics where the most probable configuration of the unloaded chain is the one where the end-to-end distance becomes zero.

2.2. Additional volumetric contribution

In Section 2.1 we have recognized that the *statistical* properties of a single chain only depend on geometrical parameters and can therefore be modelled in a relatively simple way. However, intermolecular interactions, in particular the effect of the well-known van der Waals forces, cannot be completely neglected because they are mainly responsible for the fact that rubber is almost incompressible. The action of the van der Waals forces cannot be simulated by using truss elements because the latter only serve to represent the force–stretch relation given in (4). As such they cannot undergo compressive loads. Additionally it has been observed that an arbitrary three-dimensional network of these truss elements (under tensile loading) gives us a macroscopic response where the volume enclosed by the structure is not preserved when the structure deforms. This contradicts the important experimental observation that rubber exhibits approximately incompressible behaviour. Both these difficulties are due to the fact that there is no force between the chains to keep them apart from each other as observed in reality. In order to obtain (near-) incompressible material behaviour, it is necessary to have something "between the chains". To give the structure additional volumetric stiffness, we fill the space between the chains with artificial material. The latter is modelled by means of the Helmholtz free energy function per reference volume

$$W_{\text{tetr}} = \frac{K}{4}(J^2 - 1 - 2\ln J) \tag{5}$$

where $J = \det \mathbf{F}$ denotes the determinant of the macroscopic deformation gradient $\mathbf{F}$ and K is the bulk modulus.

3. Finite element formulation

According to the introductory remarks at the beginning we establish a finite element unit cell that consists of one tetrahedral element and six truss elements lying on each edge of the tetrahedron, see also Fig. 4. The Helmholtz free energy of one unit cell then includes one contribution coming from the tetrahedral element (W_{tetr}) and another one coming from the truss elements ($W_{\text{truss } j}$, $j = 1, \ldots, 6$):

$$W = W_{\text{tetr}} + \sum_{j=1}^{6} W_{\text{truss } j} \tag{6}$$

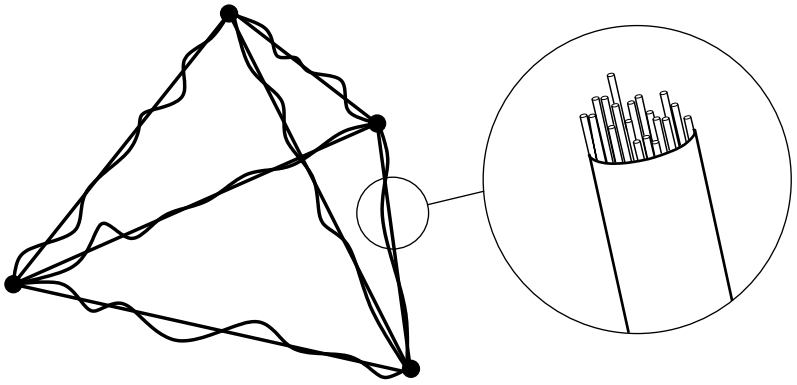

Fig. 4. Finite element unit cell with one tetrahedral element and six truss elements. Enlarged: f_{chain} chains per truss element.

In Fig. 4 a typical unit cell is shown. The straight lines represent the outline of the tetrahedral element, the truss elements are indicated by the curved lines. In reality, the number of chains per volume is huge. This fact makes it impossible to replace *each* chain by *one* truss element. Fortunately, this is not necessary because the macroscopic stress–strain behaviour is already described with sufficient accuracy if one truss element is used as representative of *several* polymer chains, i.e. a bundle of chains (see the enlargement of Fig. 4). The Helmholtz free energy function of the truss element j ($j = 1, \ldots, 6$) has then the form

$$W_{\text{truss } j} = \frac{1}{A_{0j} L_{0j}} f_{\text{chain}} W_{\text{chain } j} \tag{7}$$

with

$$W_{\text{chain } j} = k n_j \Theta \left[\frac{\lambda_{\text{chain } j}}{\sqrt{n_j}} \beta_j \gamma_j + \ln \frac{\beta_j}{\sinh \beta_j} \right] \tag{8}$$

In Eq. (7) A_{0j} is the cross-section and L_{0j} the length of the truss element in its undeformed state. As will be shown in the following derivation (see Eqs. (10)–(15)) these two quantities can be removed from the formulation. If this were not the case we would run into the difficulty to choose physically reasonable values for A_{0j} and L_{0j}. Evidently it is not possible to determine the cross-section of a chain. The length L_{0j} could be in some way related to the initial end-to-end distance r_{0j}. However, since n, l, ϑ and φ are known, such a connection would pose a restriction on the size of the elements and therefore increase the computational effort enormously. In summary, the fact that the geometry of the FE mesh (expressed in terms of L_{0j} and A_{0j}) is not directly coupled to the geometry of the polymer network can be considered to be a very advantageous feature of the model.

The parameter

$$f_{\text{chain}} = \frac{N}{N_{\text{truss}}} \tag{9}$$

defines the ratio between N, the number of polymer chains per reference volume and N_{truss}, the number of truss elements in the same reference volume. f_{chain} ranges between 1 (i.e. $N_{\text{truss}} = N$, one truss element per chain) and N (i.e. $N_{\text{truss}} = 1$, one truss element for all chains). It is clear that the aim must be to make f_{chain} as large as possible, because then the minimum number of elements and therefore maximum computational efficiency is obtained. On the other hand, convergence has to be achieved (see Section 5.4). This is the case when a decrease of f_{chain} does not alter the macroscopic result. At this point it is assumed that the chains and the trusses are approximately uniformly distributed in the structure. This justifies the assumption that N, N_{truss} and therefore also f_{chain} are constant parameters. In the case of inhomogeneous distributions of either the chains or the trusses the parameters N or f_{chain}, respectively, should be varied accordingly.

For the use of the finite element formulation we establish the weak form of the balance of linear momentum (volume forces and inertia terms neglected)

$$g = \sum_{z=1}^{n_z} g_{\text{int } z} + g_{\text{ext}} = 0 \tag{10}$$

where n_z denotes the number of finite element cells. Here $g_{\text{int } z}$ represents the virtual work of the internal forces in one unit cell, the summand g_{ext} is the contribution of the external loading. The part $g_{\text{int } z}$ is given by

$$g_{\text{int } z} = \underbrace{\int_{V_{0z}} \frac{\partial W_{\text{tetr}}}{\partial J}\delta J \,\mathrm{d}V_{0z}}_{g^{\text{tetr}}_{\text{int } z}} + \underbrace{\sum_{j=1}^{6} \int_{X_j=0}^{L_{0j}} \frac{\partial W_{\text{truss}\,j}}{\partial L_j}\delta L_j \,\mathrm{d}X_j A_{0j}}_{g^{\text{truss}}_{\text{int } z}} \tag{11}$$

where the coordinate X_j points in the longitudinal direction of the truss j, and L_j is its current length. The quantity V_{0z} denotes the volume of the unit cell (i.e. the tetrahedral element) in its undeformed state. The expression $\partial W_{\text{tetr}}/\partial J$ is equal to the hydrostatic pressure multiplied by J whereas $\partial W_{\text{truss }j}/\partial L_j$ represents the force in the truss j divided by the cross-section A_{0j}.

3.1. Truss contribution

Using (11), the second part of the latter equation is alternatively represented as

$$\sum_{j=1}^{6} \int_{X_j=0}^{L_{0j}} \frac{\partial W_{\text{truss}\,j}}{\partial L_j}\delta L_j \,\mathrm{d}X_j A_{0j} = f_{\text{chain}} \sum_{j=1}^{6} \int_{X_j=-L_{0j}/2}^{L_{0j}/2} \frac{\partial W_{\text{chain}\,j}}{\partial L_j}\delta L_j \,\mathrm{d}\left(\frac{X_j}{L_{0j}}\right) = f_{\text{chain}} \sum_{j=1}^{6} \int_{\xi_j=-1}^{1} \frac{\partial W_{\text{chain}\,j}}{\partial \lambda_{\text{chain}\,j}}\delta\lambda_{\text{chain}\,j}\frac{1}{2}\mathrm{d}\xi_j \tag{12}$$

In (12) $W_{\text{chain }j}$ is considered as a function of $\lambda_{\text{chain }j} = L_j/L_{0j}$ alone, i.e. β_j has already been replaced by the expression (3). Further, we have introduced the non-dimensional coordinate $\xi_j = X_j/(L_{0j}/2) = (2X_j)/L_{0j}$.

Inserting the stretch–displacement relation $\lambda_{\text{chain }j} = \mathbf{B}_{\text{chain }j}\mathbf{U}_z$ one finally obtains for the truss contribution of $g_{\text{int } z}$ the relation

$$g^{\text{truss}}_{\text{int } z} = \delta\mathbf{U}_z^{\mathrm{T}} f_{\text{chain}} \sum_{j=1}^{6} \int_{\xi_j=-1}^{1} \mathbf{B}^{\mathrm{T}}_{\text{chain }j} \frac{\partial W_{\text{chain }j}}{\partial \lambda_{\text{chain }j}} \frac{1}{2}\mathrm{d}\xi_j := \delta\mathbf{U}_z^{\mathrm{T}}\mathbf{R}^{\text{truss}}_z \tag{13}$$

The vector $\mathbf{U}_z$ contains the corresponding 12 degrees-of-freedom. The matrix $\mathbf{B}_{\text{chain }j}$ is given by the relation $\mathbf{B}_{\text{chain }j} = [(1 + u_{,X_j})v_{,X_j}w_{,X_j}]$ where

$$u_{,X_j} = \frac{u_{2j} - u_{1j}}{L_{0j}}, \quad v_{,X_j} = \frac{v_{2j} - v_{1j}}{L_{0j}}, \quad w_{,X_j} = \frac{w_{2j} - w_{1j}}{L_{0j}} \tag{14}$$

are the derivatives of the three displacement components u, v and w (interpolated by linear shape functions) with respect to X_j. The numbers 1 and 2 refer to the nodes 1 and 2 of the truss element, respectively.

3.2. Tetrahedral contribution

Analogously to $\lambda_{\text{chain }j} = \mathbf{B}_{\text{chain }j}\mathbf{U}_z$ the quantity J is expressed via $J = \mathbf{B}_{\text{tetr}}\mathbf{U}_z$ where the vector $\mathbf{B}_{\text{tetr}}$ is a function of the so-called tetrahedral coordinates (see e.g. Zienkiewicz and Taylor (2000, Section 8) for more details). In the finite element technology it is well-known that tetrahedral elements based on usual linear interpolation functions tend to volumetric locking in the limit of incompressibility. Different methods have been developed to avoid this phenomenon. One simple remedy against locking is the method of selective reduced integration where the volumetric part of the material response is only evaluated in the so-called centre of the element (indicated by the index 0). Such an idea can also be realized easily for the method proposed in this paper. The tetrahedral contribution of $g_{\text{int } z}$ then reads:

$$g^{\text{tetr}}_{\text{int } z} = \delta\mathbf{U}_z^{\mathrm{T}}\mathbf{B}^{\mathrm{T}}_{\text{tetr}0}\left.\frac{\partial W_{\text{tetr}}}{\partial J}\right|_0 V_{0z} := \delta\mathbf{U}_z^{\mathrm{T}}\mathbf{R}^{\text{tetr}}_z \tag{15}$$

As an additional advantage, one gains computational efficiency because the element quantities have to be evaluated only once (in the centre of the tetrahedral element).

Another possibility to circumvent the locking phenomenon is to work with higher order interpolation functions. The disadvantage of finite element simulations based on such higher order elements is the increase of the band width in the global equation system which leads to a noticeable increase of the computational effort. Alternatively so-called mixed methods (see e.g. Wriggers (2001, Section 10) for more details) or special mixed methods based on the sub-scale method (see Chiumenti et al., 2002) can be employed. In the context of the present examples it has been found that working with selective reduced integration provides satisfactory convergence behaviour. According to our present state of knowledge it is therefore not necessary to put more effort into the issue of finite element technology. This aspect should be, however, further investigated in the context of industrial applications.

After the discretization of the external loading term $g_{\text{ext}} = \delta \mathbf{U}^{\text{T}} \mathbf{F}_{\text{ext}}$, the assembling procedure and the implementation of the displacement boundary conditions one finally arrives at the non-linear equation system

$$\mathbf{G}(\mathbf{U}) := \mathbf{R}^{\text{truss}}(\mathbf{U}) + \mathbf{R}^{\text{tetr}}(\mathbf{U}) - \mathbf{F}_{\text{ext}} = \mathbf{0} \tag{16}$$

where $\mathbf{U}$ represents the global nodal displacement vector and $\mathbf{R}^{\text{truss}}$ ($\mathbf{R}^{\text{tetr}}$) the global residual force vector of the truss (tetrahedral) contribution.

4. Micro–macro transition

It is important to state clearly at which point the micro–macro transition takes place. In Section 2 the chain stretch λ_{chain} has been defined as the ratio between the current end-to-end distance r and the end-to-end distance r_0 in the undeformed state of the network. At the finite element level we compute $\lambda_{\text{chain}\,j}$ by means of the quotient L_j/L_{0j}. We therefore obtain the important connection

$$\lambda_{\text{chain}\,j} = \frac{L_j}{L_{0j}} = \frac{r_j}{r_{0j}} \tag{17}$$

between the micro scale (quantities r_j, r_{0j}) and the macro scale (quantities L_j, L_{0j}). We can also draw the crucial conclusions that

(i) the current length L_j of the truss element is in general *not* equal to the end-to-end distance r_j of the chain,
(ii) the truss lengths L_{0j} can be chosen *independently* of the chain geometry.

5. Numerical simulations

The aim of this section is to study how the deformation behaviour of the network deviates from the one of the single chain. For this purpose we generate a finite element mesh with 37116 truss elements per mm^3 and choose the boundary conditions suitably to model homogenous deformation states. Fig. 5(a) shows the undeformed and (b) the deformed mesh for uniaxial tension. The parameters for these calculations read $n = 30$, $\gamma = 1$, $N = 1.910 \times 10^{21}\ \text{mm}^{-3}$, $f_{\text{chain}} = 5.146 \times 10^{16}$ ($N_{\text{truss}} = 37116\ \text{mm}^{-3}$), $K = 10^5\ \text{N/mm}^2$, $\text{TA} = 10$, $k = 1.380662 \times 10^{-20}\ \text{N mm/K}$ and $\Theta = 273\ \text{K}$. It should be emphasized that the values of n, γ (ϑ, φ) and N are known immediately when the components of the polymer mixture are known. The Boltzmann's constant k is certainly fixed, too. We further consider only isothermal processes ($\Theta = \text{const.}$). To enforce (near-)incompressibility, the bulk modulus K which plays the role of a penalty parameter has to be chosen as large as possible. The only user-defined parameter is the ratio $f_{\text{chain}} = N/N_{\text{truss}}$ or, alternatively, the number of truss elements per reference volume N_{truss}.

5.1. General network behaviour

To understand the network behaviour it is instructive to look at the chain stretch distribution for various deformation cases, e.g. pure shear ($\lambda_1 = \lambda$, $\lambda_2 = 1$ and $\lambda_3 = 1/\lambda$) and uniaxial compression.

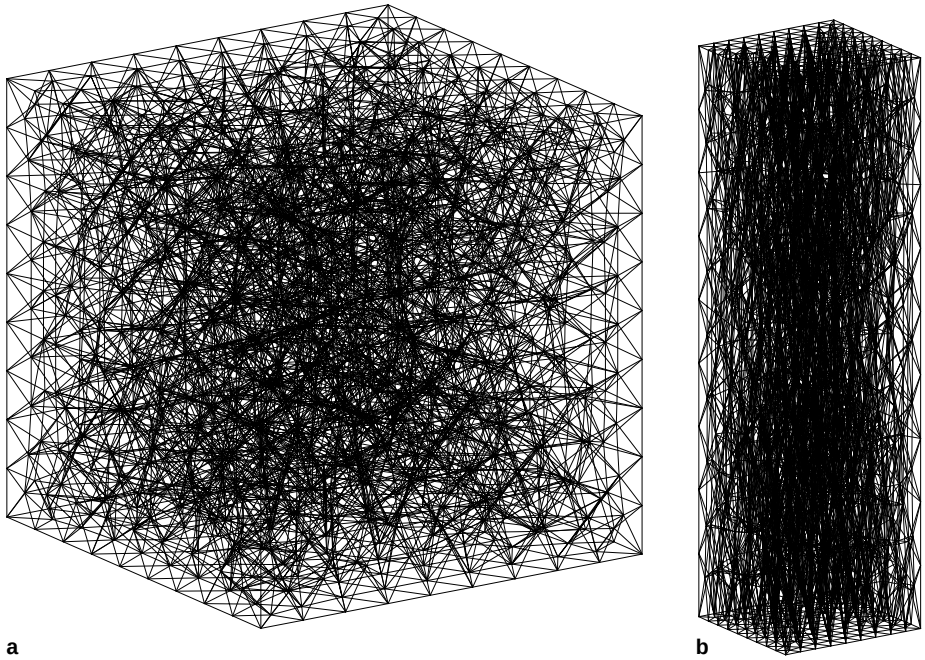

Fig. 5. Typical FE mesh (1 mm × 1 mm × 1 mm), here with 37116 truss elements: (a) undeformed mesh, (b) deformed mesh in uniaxial tension (scaled).

In the pure shear experiment the average truss length is calculated to read $L_{\text{aver}} = 0.137$ mm. The stretch values of the chain bundles are plotted in Fig. 6(a) ($\lambda_{\text{network}} = 5$: $\lambda_{\text{chain aver}} = 2.56$, $\lambda_{\text{network}} = 9$: $\lambda_{\text{chain aver}} = 4.42$). The result is obvious. An increase of the prescribed network stretch must lead to an increase of the average chain stretch $\lambda_{\text{chain aver}}$ in this case. Due to the unstructured discretization the chain stretch distribution becomes at the same time more diverse.

Secondly we perform the simulation of uniaxial compression. Due to the fact that the material is almost incompressible the chains perpendicular to the loading direction are stretched whereas the chains in loading direction are compressed. The load is taken by the tetrahedral elements. In the perpendicular direction the macroscopic stress contribution coming from the tetrahedral elements has the same absolute value as the macroscopic stress resulting from the tension of the chains. Since the signs of the two stress contributions are, as expected, different, the total macroscopic stress in this direction vanishes. The average stretch in the single chains is significantly smaller than in the other examples ($\lambda_{\text{network}} = 0.15$: $\lambda_{\text{chain aver}} = 2.03$), see Fig. 6(b).

The behaviour of the chains for the load case uniaxial compression is additionally visualized by means of the angle α which is defined as the angle between the truss element and the plane perpendicular to the loading direction. Fig. 7(a) shows the angle distribution in the undeformed state (crosses) and the deformed state (bars) of a uniaxial compression simulation. In the undeformed case a relatively uniform distribution is seen. This changes when the load is applied. Then the number of small angles, especially $\alpha = 0$, becomes much larger, i.e. the number of chains which are lying perpendicular to the loading direction increases. These chains are loaded with higher forces, see Fig. 7(b).

5.2. Influence of TA on the macroscopic material behaviour

The dependence of the network response on number of terms in the inverse Langevin function is studied in Figs. 8(a) and (b), 9(a) and (b) where the deformation states uniaxial tension, biaxial tension, pure shear and uniaxial compression, respectively, have been considered. If only one term in the series expansion is used (TA = 1) the curve exhibits Neo-Hooke-like material behaviour. If TA is clearly larger than one, the classical S-shaped function is obtained (Ogden-like material behaviour). This is especially visible in the case of uniaxial tension.

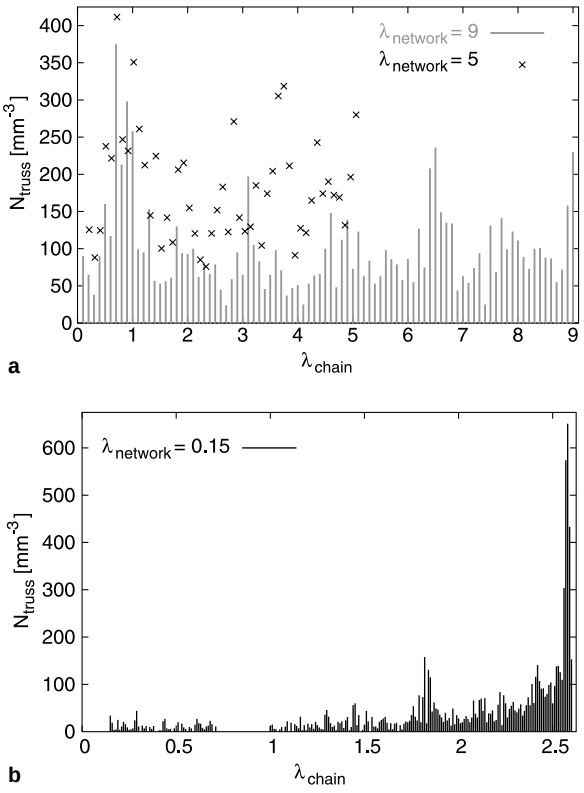

Fig. 6. Chain stretch distributions: (a) pure shear, (b) uniaxial compression.

The curve for uniaxial compression (Fig. 9(b)) is significantly different from the other three. This can be explained by the fact that the average stretch in the single chains is much smaller than in the other examples ($\lambda_{\text{network}} = 0.15$: $\lambda_{\text{chain aver}} = 2.03$), see Fig. 9(b). Therefore the macroscopic response is in this case practically independent of TA.

In summary, TA should be large enough to yield a converged solution. Fig. 8(a) shows that 10 terms are usually enough. The choice of TA = 1 is special in the regard that then a Neo-Hooke material is obtained. However, the latter model is not realistic for large stretches.

Further it is important to note that, independently of TA, the macroscopic stress vanishes for $\lambda_{\text{network}} = 1$ as expected from the physical point of view. The fact that the chain force does not vanish for $\lambda_{\text{chain}} = 1$ does not have a non-physical effect on the network response.

5.3. Interaction between the micro and the macro structure

One of the advantages of the present model is the possibility to transfer the information from the micro level to the macro level and contrariwise. The possibility to obtain the information of both levels during a calculation leads to a better understanding of the mechanical behaviour of rubber-like materials.

5.3.1. Influence of the chain length

The first interesting issue is the dependence of the macroscopic material response on the chain length. In Fig. 10 an undeformed chain (end-to-end distance r_0) consisting of six chain segments is shown ($n = 6$).

The calculation of the real chain length is certainly very complex and difficult because every polymer chain has random shape, to be expressed in terms of the number of links n and varying segment lengths and rotation angles. Using the assumptions that (i) all segments have the same length and (ii) the valence angle δ and the rotation angle φ are constant within one chain, the end-to-end distance of the chain in the undeformed state can be computed with the relation (2): $r_0 = l\sqrt{n}\gamma$, see Flory (1969).

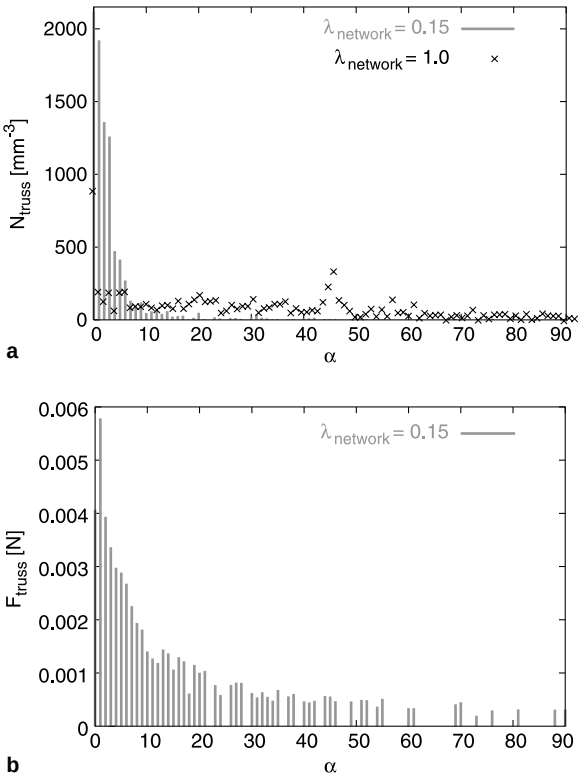

Fig. 7. Uniaxial compression simulations: (a) angle distribution for the loaded and the unloaded case, (b) force distribution depending on the angle α.

Among the three parameters l, n and γ which control the initial chain length r_0 only the quantities n and γ enter the Helmholtz free energy function W_{chain}. Thus the finite element result is independent of l. In other words, using the same finite element discretization and boundary conditions for a group of polymer networks defined by the prescribed parameters n, γ, N and an arbitrary segment length l leads to the same results, i.e. the same chain stretches $\lambda_{\text{chain}\,j}$ in each truss element. Certainly the resulting current chain lengths computed by $r_j = \lambda_{\text{chain}\,j}(l\sqrt{n}\gamma)_j$ depend again on l.

In contrast, the finite element solution depends noticeably on the choice of γ and n. For $\varphi = 90°$ and decreasing ϑ the value of γ increases. This means practically that r_0 increases if all other chain properties are left unchanged. Considering the same argument as used in Section 2.2 (see also Figs. 2 and 3) it can be expected that the stiffness of the polymer network increases, see Fig. 11. The simulation has been based on the parameters $n = 10$, $N = 2.071 \times 10^{22}\ \text{mm}^{-3}$, $f_{\text{chain}} = 2.329 \times 10^{18}$ ($N_{\text{truss}} = 8892\ \text{mm}^{-3}$), $K = 10^6\ \text{N/mm}^2$ and $\text{TA} = 10$.

Another method to influence the initial chain length is to modify the parameter n. In Fig. 1(a) it has been observed that the chain stiffness increases with decreasing n. Note that this effect cannot be explained by means of the truss analogy discussed in Section 2.1. It is rather a non-linear effect caused by the statistical properties of the polymer chains. Again the polymer network exhibits a behaviour similar to the single chain, see Fig. 12. The stiffness of the network decreases with increasing n.

It should also be emphasized that in the limit $n \to \infty$ a Neo-Hooke-like curve is obtained whereas a moderate n leads to a S-shaped stress–stretch function. Similar behaviour has been observed in the context of a varying TA, see Section 5.2.

5.3.2. Non-affinity

Most network models are based on the assumption of affinity. It means that the length of a single chain is changing to the same extent as the dimension of the whole network. In Fig. 13 a pure shear deformation state

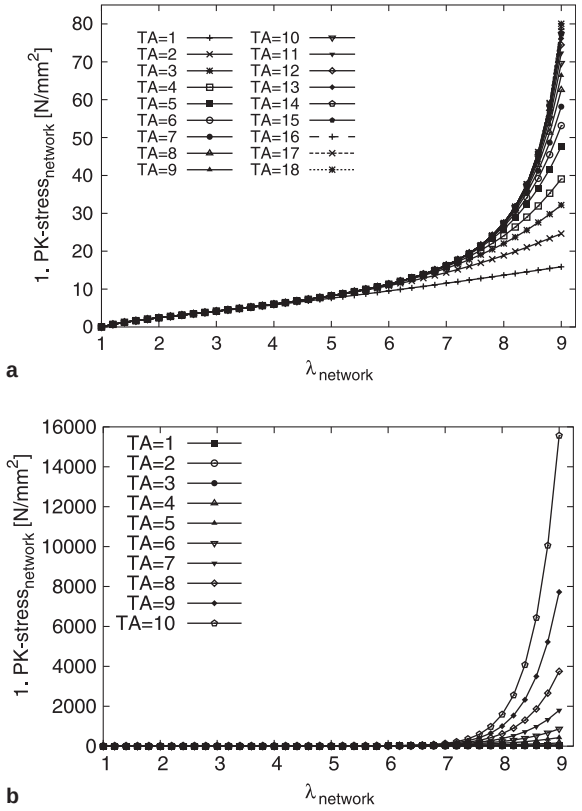

Fig. 8. Influence of TA: (a) uniaxial tension, (b) biaxial tension.

($\lambda_1 = \lambda$, $\lambda_2 = 1/\lambda$, $\lambda_3 = 1$) has been applied. If the four-chain network obeys affinity all four chains undergo the stretch $\lambda_{\text{chain}} = \sqrt{(1+\lambda^4)}/(\lambda\sqrt{2})$, i.e. all four chains are equally long and the centre point stays in the centre of the specimen, independently of the size of λ.

In the present model it is easily possible to deviate from affinity. If two chain bundles (truss elements) undergo the same stretch λ_{chain} their end-to-end distances can be different:

$$\lambda_{\text{chain 1}} = \frac{r_1}{l_1\sqrt{n_1}\gamma_1} = \frac{r_2}{l_2\sqrt{n_2}\gamma_2} = \lambda_{\text{chain 2}} \Rightarrow r_1 = \frac{l_1\sqrt{n_1}\gamma_1}{l_2\sqrt{n_2}\gamma_2} r_2 \tag{18}$$

Conversely, if the macroscopic deformation is prescribed in such a way that for geometrical reasons two chain groups must have the same end-to-end distance $r_1 = r_2$, this does not necessarily require $\lambda_{\text{chain 1}} = \lambda_{\text{chain 2}}$. Thus, as stated above, we are able to model non-affine deformation if different values of n or γ are incorporated into the FE model.

To illustrate non-affine deformation behaviour we look at the smallest possible network consisting of eight truss elements (see Fig. 14) and perform uniaxial tension simulations by using the following parameters: $\gamma = 1$, $N = 7.975 \times 10^{16}\ \text{mm}^{-3}$, $f_{\text{chain}} = 9.968 \times 10^{15}$ ($N_{\text{truss}} = 8\ \text{mm}^{-3}$), $K = 10^6\ \text{N/mm}^2$ and TA = 7.

In the first simulation we select for every chain bundle the same number of links ($n = 8$). As expected the deformation of the network is affine. In the second simulation we work with the distributions 1 and 2, see the inset of Fig. 14(a). The dotted lines represent chains where n is chosen to be equal to 4 whereas the chains plotted as solid lines have 12 chain links ($n_{\text{aver}} = 8$). The average number of segment links amounts in both cases to 8.

Only for distribution 1 the resulting deformation turns out to be non-affine. For symmetry reasons distribution 2 leads to an affine deformation. The stress–stretch curve agrees with the one for $n = \text{const.} = 8$. The network response is much stiffer than in the simulation based on distribution 1 although the same average

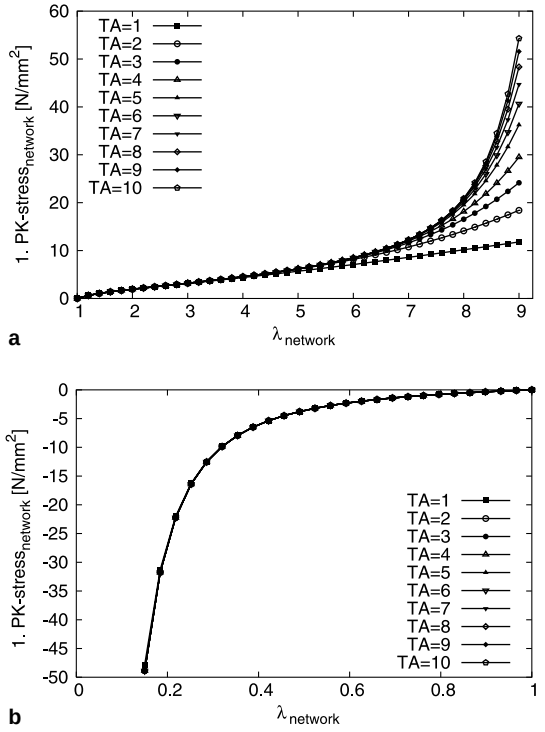

Fig. 9. Influence of TA: (a) pure shear, (b) uniaxial compression.

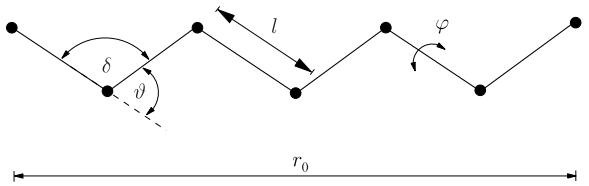

Fig. 10. Idealized chain with six segments.

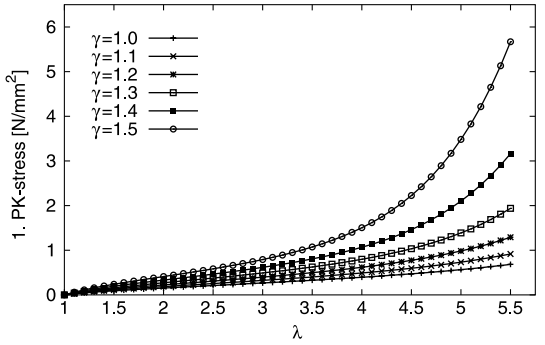

Fig. 11. Uniaxial tension simulations: variation of γ.

value for n has been used. This can be explained by a simple linear consideration (see Fig. 15). Distribution 1 can be described by means of two pairs of parallel springs which are in series (see Fig. 15(a)). For the first pair

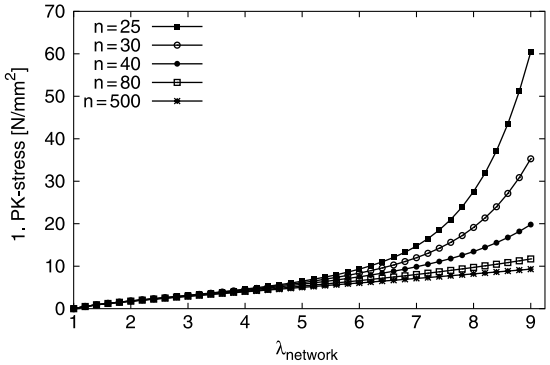

Fig. 12. Uniaxial tension simulations: variation of n.

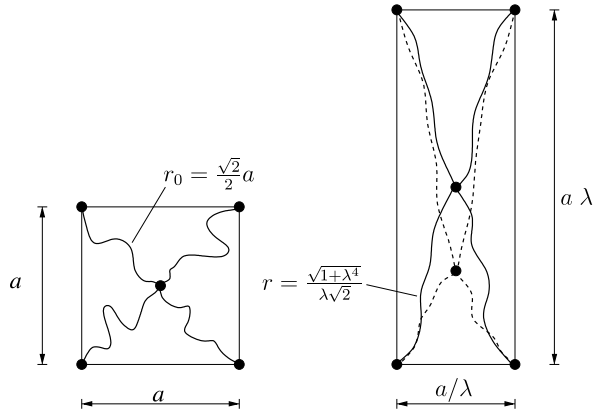

Fig. 13. Affine (solid lines) and non-affine (dashed lines) deformation.

we obtain the stiffness $c_{\bigstar} = 2c_1$, the second pair yields $c_{\bigstar} = 2c_2$. The spring pairs in series yield the total stiffness $c_{\text{tot1}} = 2c_1c_2/(c_1 + c_2)$. For distribution 2 we have two springs in parallel: $c_{\bigstar} = c_1 + c_2$. The two springs with the stiffness $c_{\bigstar}$ can be considered to be in series. We then obtain a total stiffness of $c_{\text{tot2}} = (c_1 + c_2)/2$. Inserting $c_1 = 4$ and $c_2 = 12$ leads to $c_{\text{tot1}} = 6$ and $c_{\text{tot2}} = 8$, i.e. the second configuration yields the stiffer response. A similar observation is made in the non-linear case where the differences between the curves for the two distributions are relatively large.

In the two last simulations the value of n has been varied over a certain range, in the first case from $n_{\min} = 3$ to $n_{\max} = 21$ (distribution 3), in the second case from $n_{\min} = 3$ to $n_{\max} = 11$ (distribution 4). The average value of n (n_{aver}) is in both cases equal to 8. As expected, the former case leads to a more distinct deviation from affinity, the material response is stiffer than in the simulation with the smaller range of n ($3 \leqslant n \leqslant 11$).

It is further interesting to investigate how different distributions of n influence the behaviour of more complex polymer networks. In comparison to the previous set of parameters we change only the discretization. We have now $f_{\text{chain}} = 8.968 \times 10^{12}$ ($N_{\text{truss}} = 8892\ \text{mm}^{-3}$). The results are shown in Fig. 14(b). Four different kinds of distributions are tested: (1) $n = \text{const.} = 8$, (2) two chain groups, $n_{\text{aver}} = 8$, (3) diverse distribution with $5 \leqslant n \leqslant 20$ ($n_{\text{aver}} = 8$), (4) diverse distribution with $5 \leqslant n \leqslant 200$ ($n_{\text{aver}} = 8$). The results for the distributions (1), (2) and (3) are almost equal and approximately affine. The curve (4) deviates from the other three, it shows a slightly stiffer response. In comparison to the observations made at the coarse network it can be said that the more complex network reacts much more insensitively to inhomogeneities in the chain distribution. Obviously the influences of high and low values of n balance each other in complex chain configurations. For this reason the range of n has to be very large in order to achieve a significant influence on the stress–stretch response.

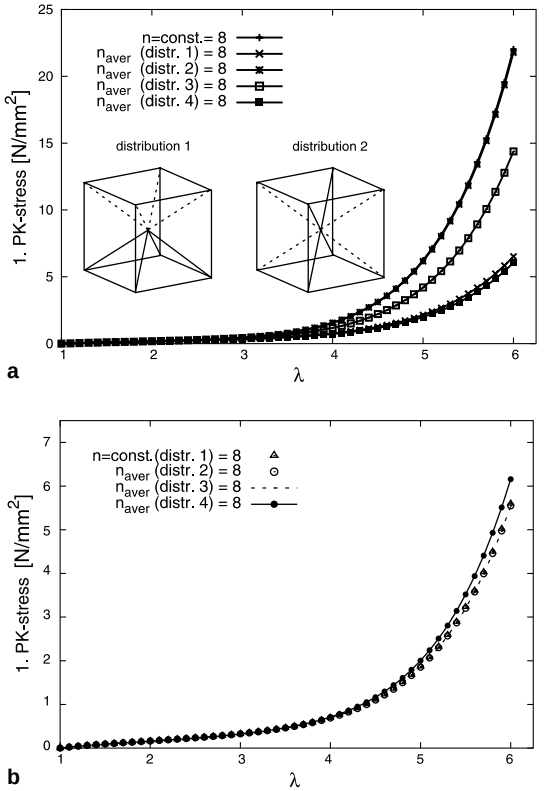

Fig. 14. Influence of n for uniaxial tension simulations: (a) network with eight trusses, (b) network with 8892 trusses.

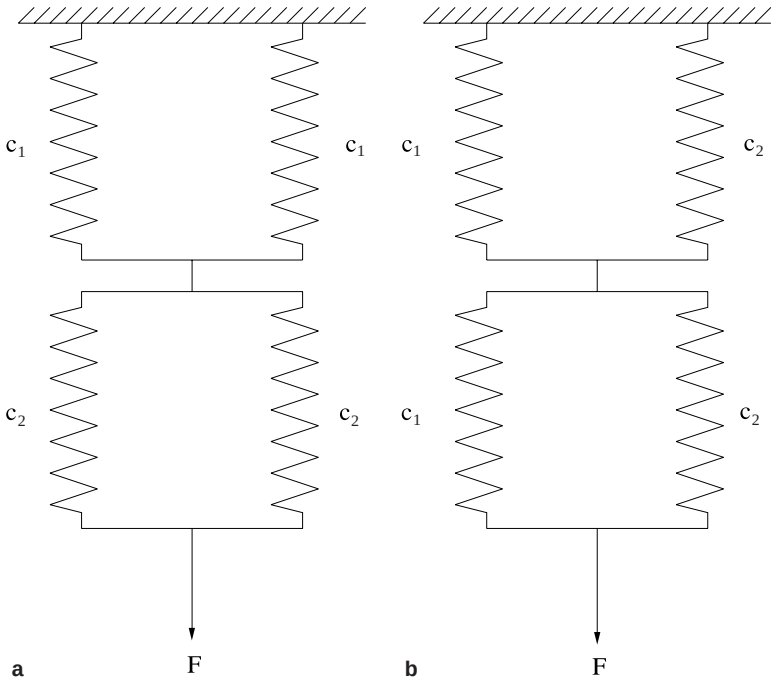

Fig. 15. Different stiffnesses: (a) distributions 1, (b) distribution 2.

5.3.3. Influence of an inhomogeneous chain bundle arrangement

Non-affine behaviour can also be generated artificially by working with an inhomogeneous chain bundle arrangement. Practically this means that the truss elements are not uniformly distributed in the structure but concentrated on a certain domain. In order to investigate this influence four uniaxial tension tests were simulated with different finite element discretizations, see the insets of Fig. 16(a)–(d). The degree of inhomogeneity increases from (a) to (d). The following parameters were used: $n = 9.5$, $\gamma = 1$, $N = 3.793 \times 10^{22}\,\mathrm{mm}^{-3}$, $f_{\mathrm{chain}} = 3.230 \times 10^{17}$ ($N_{\mathrm{truss}} = 117420\,\mathrm{mm}^{-3}$), $K = 10^6\,\mathrm{N/mm}^2$, $\mathrm{TA} = 5$. The results of the simulations are shown in Fig. 17. Interestingly the stiffness of the material on the macro level decreases with increasing degree of inhomogeneity.

The explanation of this phenomenon is similar to the one given in Section 5.3.2. Let us consider a unit cube (side length equal to 1 mm) which is divided into two equal parts arranged above each other. We put 200 chains and 100 truss elements into this cube ($N = 200\,\mathrm{mm}^{-3}$, $N_{\mathrm{truss}} = 100\,\mathrm{mm}^{-3}$) and introduce a parameter a ($0 < a < 1$) to describe how the trusses are distributed among the two sub-structures:

$$N_{\mathrm{truss}\ 1} = aN_{\mathrm{truss}}, \quad N_{\mathrm{truss}\ 2} = (1-a)N_{\mathrm{truss}} \tag{19}$$

It is assumed that the chains are distributed approximately homogeneously. The value of N is therefore constant. The ratios $f_{\mathrm{chain}\ 1}$ and $f_{\mathrm{chain}\ 2}$ are then computed with

$$\begin{aligned} f_{\mathrm{chain}\ 1} &= \frac{N}{N_{\mathrm{truss}\ 1}} = \frac{1}{a}\frac{N}{N_{\mathrm{truss}}} = \frac{1}{a} f_{\mathrm{chain}} \\ f_{\mathrm{chain}\ 2} &= \frac{N}{N_{\mathrm{truss}\ 2}} = \frac{1}{1-a}\frac{N}{N_{\mathrm{truss}}} = \frac{1}{1-a} f_{\mathrm{chain}} \end{aligned} \tag{20}$$

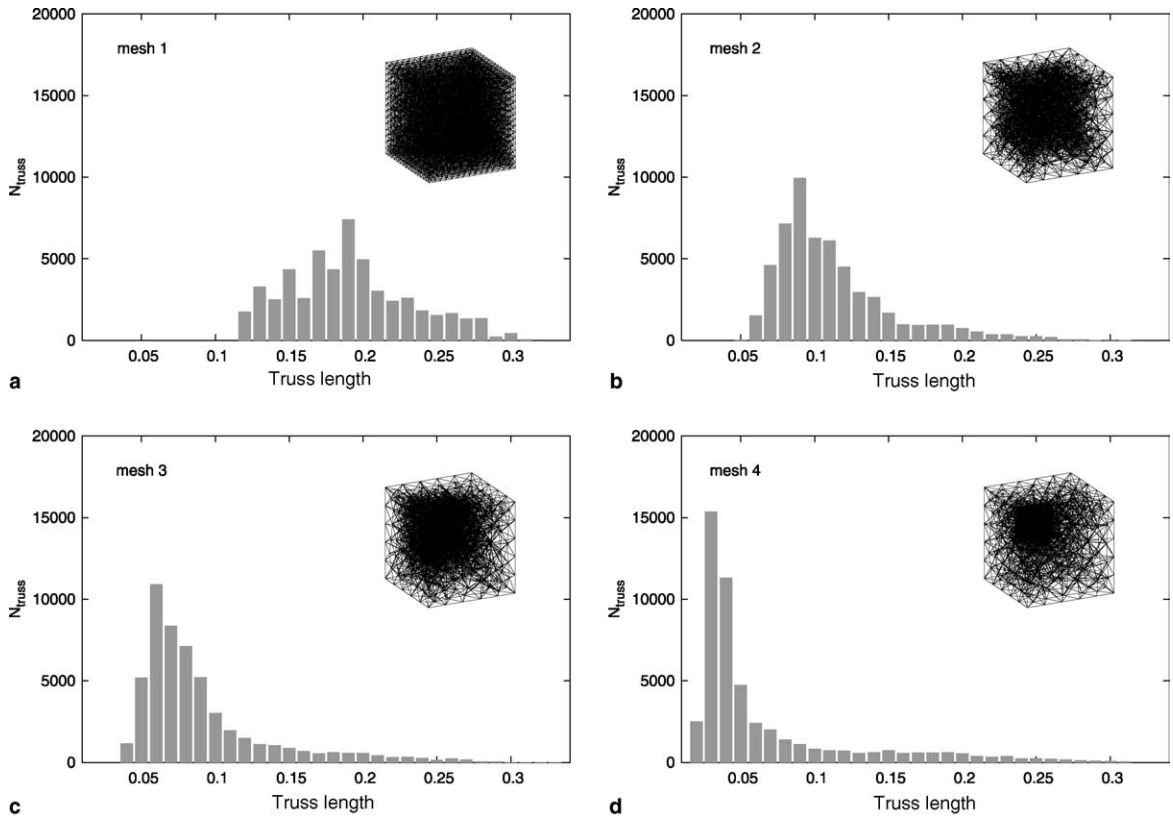

Fig. 16. Truss length distributions of four different meshes with different inhomogeneities. Inset: undeformed meshes.

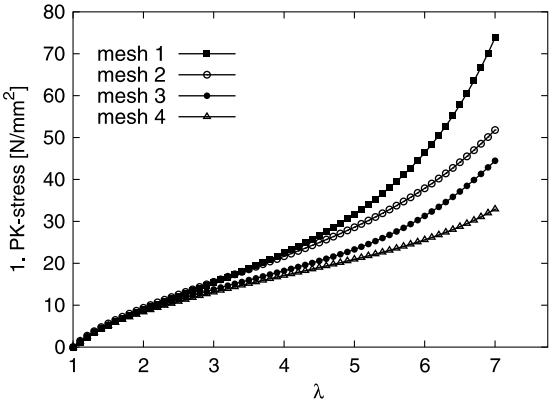

Fig. 17. Uniaxial tension simulations for four meshes with different inhomogeneity.

In order to account correctly for the inhomogeneous chain bundle arrangement it would be necessary to work domainwise with different values of f_{chain}. Instead, f_{chain} has been held constant in the simulation. Referring to our simple example this means that in the first sub-structure we obtain $N_1 = f_{\text{chain}} N_{\text{truss }1} = (N/N_{\text{truss}}) a N_{\text{truss}} = aN$. For the second structure we compute the value $N_2 = f_{\text{chain}} N_{\text{truss }2} = (1-a)N$. The chain densities N_1 and N_2 can be seen to be proportional to the stiffnesses of the sub-structures. If these are interpreted as springs, they act in series, i.e. the resulting stiffness must be proportional to $a(1-a)N$. The function $a(1-a)$ has a maximum at $a = 0.5$. For this reason the homogeneous chain bundle arrangement ($a = 0.5$) yields the highest stiffness. The closer a approaches 0 or 1, respectively, the softer is the material behaviour at the macro level.

It can be concluded that in meshes with strongly varying element sizes the parameter f_{chain} should be adapted according to the mesh density. It is then not suitable to treat it as a constant. One possibility is to split the mesh into various regions which are characterized by a certain mesh density (N_{truss}). Knowing the value of N the parameter f_{chain} can be computed for each region separately. Note again that f_{chain} represents the number of chains in one chain bundle (truss element). In this way using a varying f_{chain} in an approximately homogeneous mesh serves to model a varying chain density inside a structure.

5.4. Studies of convergence

It has been mentioned before that the ratio f_{chain} is certainly a crucial indicator for the computational effort. An increase of f_{chain} means a decrease of the number of elements. Although the proposed FE approach has the important advantage that (besides f_{chain}) only physically based parameters are used, it would not be very useful if the element density exceeded by far the one of conventional finite element calculations (based on continuum mechanical material laws). The purpose of the present section is therefore to study the macroscopic stress–stretch behaviour in dependence of f_{chain}. We stress the fact that such an investigation is only useful if the stress or strain state, respectively, is *not* homogeneous. Otherwise every unit cell exhibits (approximately) the same deformation state. Obviously then the macroscopic result is (almost) independent of the number of elements and consequently also independent of f_{chain} (see Figs. 18 and 19).

5.4.1. Block under compression

The first inhomogeneous example is a block under compression, see the inset in Fig. 20. The input parameters for this simulation read: $n = 10$, $\gamma = 1$, $N = 2.266 \times 10^{19}\ \text{mm}^{-3}$, $K = 10^6\ \text{N/mm}^2$ and $\text{TA} = 1$. Fig. 21 shows the deformed mesh including the truss forces ($N_{\text{truss}} = 22\,050\ \text{mm}^{-3}$). In Fig. 20 the load–compression curves obtained with different meshes ($2754\ \text{mm}^{-3} \leqslant N_{\text{truss}} \leqslant 87\,060\ \text{mm}^{-3}$, f_{chain} changed accordingly) are plotted. The compression level is computed with $c = w/H$, where w is the maximum displacement measured at point A, see the inset in Fig. 20, and H denotes the height of the block. The variable $v = p/p_0$ represents

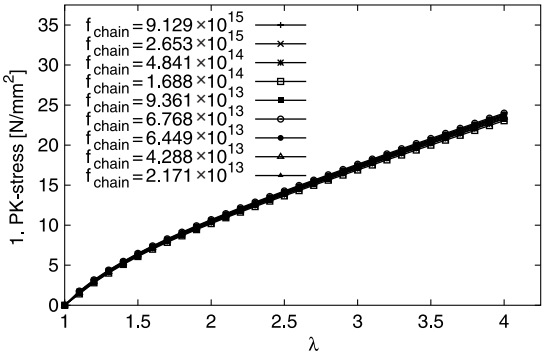

Fig. 18. Study of convergence using uniaxial tension simulations: Neo-Hooke-like material behaviour.

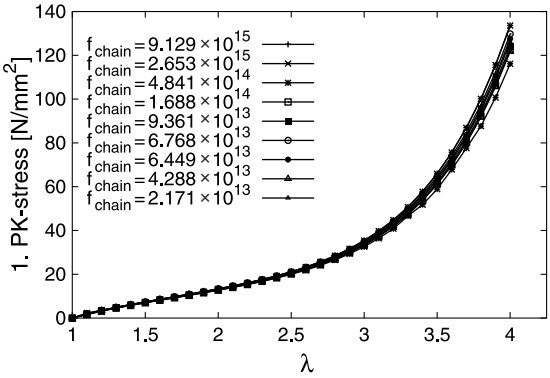

Fig. 19. Study of convergence using uniaxial tension simulations: Ogden-like material behaviour.

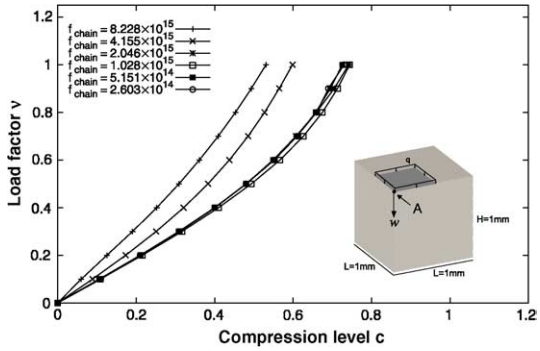

Fig. 20. Study of convergence: calculations for different meshes. Inset: system description.

the load factor where the reference value was chosen to be $p_0 = 450$ N/mm^2. The calculations show good convergence behaviour with increasing number of elements (see Fig. 20).

5.4.2. Inhomogeneous simple shear

In the second example the finite element simulation of simple shear has been carried out. Again, different meshes were used, varying from $N_{\text{truss}} = 600$ mm^{-3} to $N_{\text{truss}} = 37116$ mm^{-3}. The computation is based on the input parameters $n = 10$, $\gamma = 1$, $N = 2.011 \times 10^{19}$ mm^{-3}, $K = 10^6$ N/mm^2 and TA $= 1$. Fig. 22 shows the chain

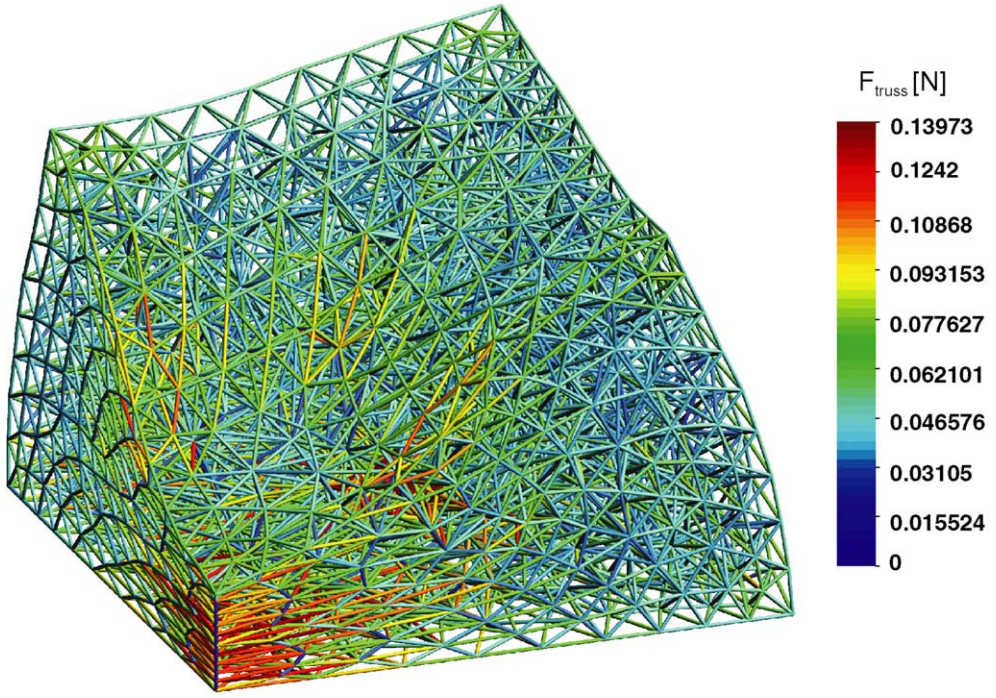

Fig. 21. Study of convergence: deformed FE-mesh with truss forces.

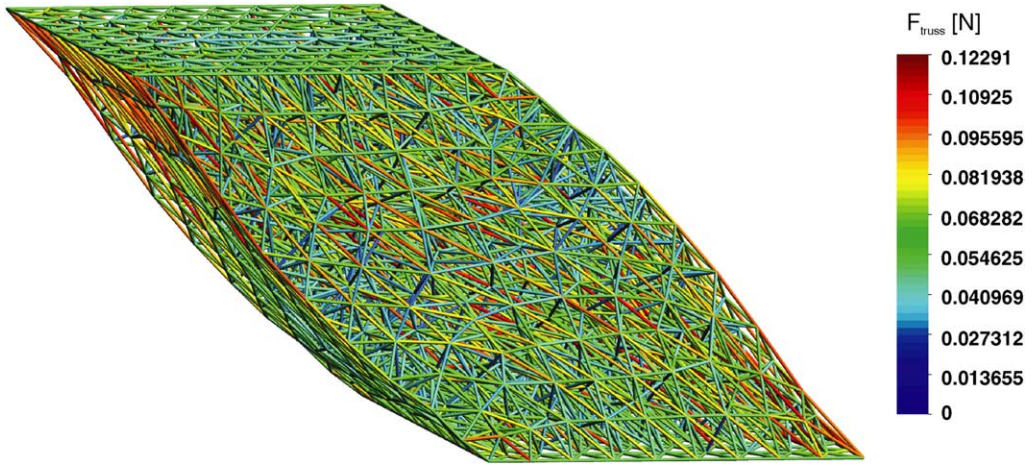

Fig. 22. Study of convergence: deformed FE-mesh with truss forces.

forces in the deformed mesh ($N_{\text{truss}} = 23\,520\ \text{mm}^{-3}$). The convergence with increasing number of elements, see Fig. 23, is even better than in the first example. This can be explained by the fact that the shear deformation is by definition approximately volume-conserving. Therefore the locking effect which in the present examples is caused by the constraint of (near-)incompressibility ("volumetric" locking) does not have such a serious influence as in the first example. In summary, it may be stated that we are able to simulate inhomogeneous deformation states with a computational effort comparable to conventional computations. So, the present approach should also be suitable for industrial applications. Note again that its main advantage is that the fit of any

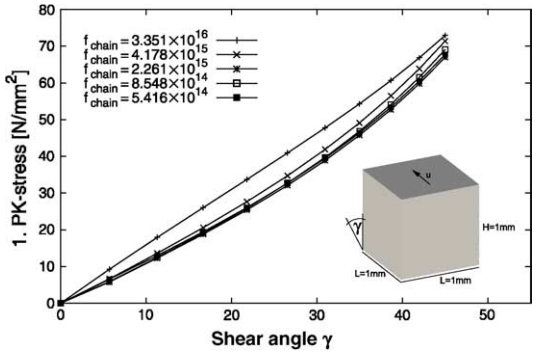

Fig. 23. Study of convergence: calculations of different meshes. Inset: system description.

material parameters is not necessary if the polymer chemist is able to provide the ''micro mechanical'' parameters n, N, ϑ and φ.

5.4.3. Rubber boot

In Fig. 24 the half of a rubber boot is shown. The boot is bounded by two rigid steel plates. The lower plate is hold fixed. The vertical displacement u and the rotation φ of the upper steel plate are controlled.

Fig. 25 shows the deformed system of the rubber boot simulated by means of the present approach.

Figs. 26 and 27 show studies of convergence obtained with the present and an alternative continuum mechanical model, respectively. The material parameters for the models read (I) present approach: $n = 40$, $\gamma = 1$, $N = 1.804 \times 10^{17}$ mm^{-3}, $K = 10^6$ N/mm^2, (II) continuum model: $\mu = 0.68$ N/mm^2 and $K = 10^6$ N/mm^2. In both cases, Neo-Hooke-like material behaviour (TA) is assumed.

The convergence behaviour is very similar. In both computations 6250 tetrahedral elements or unit cells, respectively, are sufficient to obtain a converged solution. The shorthand notation ''u–p'' refers to a two-field mixed element formulation. It should be also emphasized that these meshes include the same number of degrees-of-freedom because the nodes of the truss elements are connected to the ones of the tetrahedral elements and therefore do not introduce additional degrees-of-freedom into the system. It can be therefore concluded that the new approach does not require finer meshes, even if complex, practically relevant structures are considered.

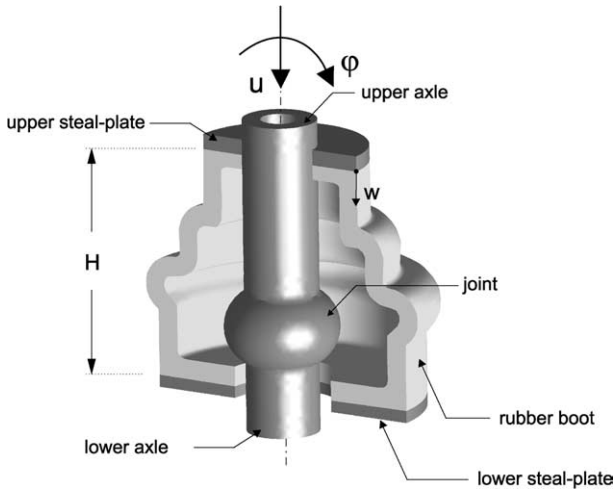

Fig. 24. Rubber boot: description of the system.

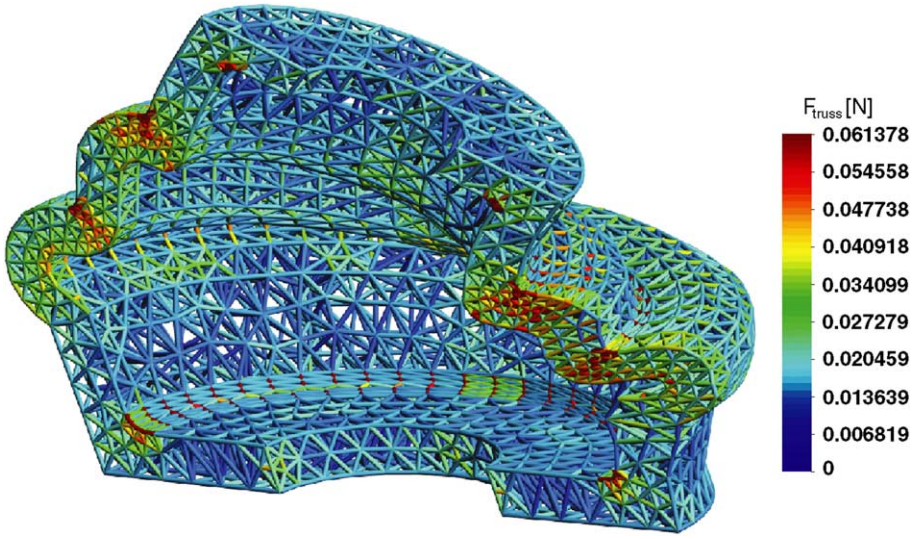

Fig. 25. Rubber boot under compression and bending load.

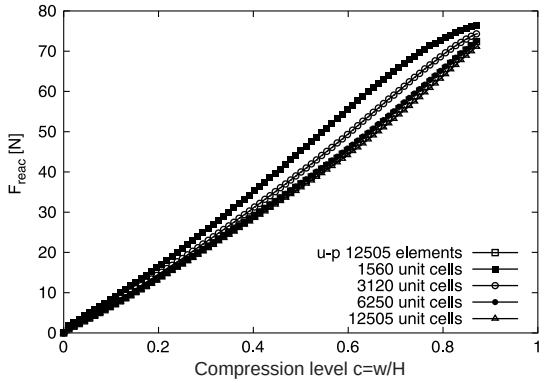

Fig. 26. Study of convergence: present model.

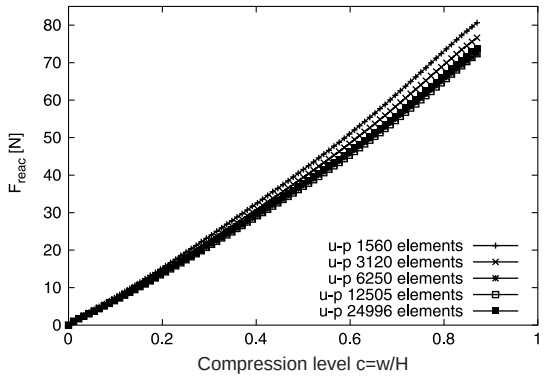

Fig. 27. Study of convergence: continuum mechanical model.

6. Validations

6.1. Comparison of the proposed approach with continuum-based models and with Treloar's data

In this section we compare the results of the proposed approach and well-known continuum-based material laws on the basis of experimental measurements. The present concept should not be considered as a new *model* because the micro mechanical basis is not different from the one e.g. taken by Arruda and Boyce (1993). However, it offers the possibility to include non-affinity, arbitrary chain arrangements and finally inelastic material behaviour. Prerequisite for these extensions is the validation of the concept by means of experimental results.

For the first comparison the data of Treloar for vulcanized rubber (Treloar, 1944) are used. In that work three deformation states were investigated: uniaxial tension, pure shear and biaxial tension. Our aim is to find *one* material parameter set which fits all three experiments with satisfactory agreement. We compare the proposed approach with the following continuum mechanical material laws, see Table 1. Note that in all calculations the penalty method is used to enforce (near-) incompressibility. Due to the fact that we do not present the continuum models in the volumetric–deviatoric decoupled form, the penalty parameter is here not the bulk modulus K but the Lamé constant Λ. A reasonable choice for it is 1000 N/mm^2. In addition, the models include different numbers of material parameters. In the fitting procedure all three deformation states are taken into account simultaneously. For the optimized material parameters see Table 1. The parameters of the present approach (abbreviated from now on as BR) have been identified to read $n = 5.1$, $\gamma = 1$, $N = 7.975 \times 10^{16}$ mm^{-3}, $K = 10^6$ N/mm^2 and TA $= 7$. For the simulations we use 8892 truss elements per mm^3, i.e. the value $f_{\text{chain}} = 8.968 \times 10^{12}$ ($N_{\text{truss}} = 8892$ mm^{-3}) is obtained.

At first we compare the uniaxial tension simulations (see Fig. 28). Here the Neo-Hooke and the Mooney–Rivlin models are not satisfactory in the domain of large stretches, i.e. they are not able to mirror the classical S-shape behaviour. The AB model (although it has also only two parameters) reproduces the material response very well. The results of BR are, as expected, very similar to the ones of AB. The Yeoh model shows an explicit S-shape but yields a slightly too stiff behaviour in the large stretch domain. The best agreement with the experiment is here obtained by means of the Ogden model.

The results of the pure shear test are plotted in Fig. 29. Again the Neo-Hooke and the Mooney–Rivlin models are not able to simulate the S-shape and consequently do not show a good agreement with the experimental data. AB and BR show similar behaviour and are able to mirror the experimental data in a satisfactory manner. The curve for the Yeoh model lies in the entire stretch range above the experimental values. Again the Ogden model yields a very good agreement.

The last experiment to be investigated is the biaxial tension test. The results are plotted in Fig. 30. The Neo-Hooke model is, as in the other test cases, not able to capture the S-shape. The Mooney–Rivlin model

Table 1
Different strain energy functions with optimized parameters

Model	Strain energy function	Parameters
Neo-Hooke (Treloar, 1943)	$W = \frac{\mu}{2}(\lambda_1^2 + \lambda_2^2 + \lambda_3^2 - 3) - \mu \ln J + \frac{\Lambda}{4}(J^2 - 1 - 2\ln J)$	$\mu = 0.377$ N/mm^2
Arruda and Boyce (1993)	$W = \mu \sum_{i=1}^{5} \frac{C_i}{n^{2i-2}}(I_1^i - 3^i) + \frac{\Lambda}{4}(J^2 - 1 - 2\ln J)$	$\mu = 0.30$ N/mm^2
	$C_{1,2,3,4,5} = \frac{1}{2}, \frac{1}{20}, \frac{11}{1050}, \frac{19}{7050}, \frac{519}{673750}$	$n = 25.9$
Mooney (1940) and Rivlin (1948)	$W = C_{10}(I_1 - 3) + C_{01}(I_2 - 3) + \frac{\Lambda}{4}(J^2 - 1 - 2\ln J)$	$C_{10} = 0.16$ N/mm^2 $C_{01} = 0.01$ N/mm^2
Yeoh (1993)	$W = \sum_{i=1}^{3} C_{i0}(I_1 - 3)^i + \frac{\Lambda}{4}(J^2 - 1 - 2\ln J)$	$C_{10} = 0.1993$ N/mm^2 $C_{20} = -0.0015$ N/mm^2 $C_{30} = 0.000037$ N/mm^2
Ogden (1972)	$W = \sum_{i=1}^{3} \left[\frac{\mu_{(i)}}{\alpha_{(i)}}(\lambda_1^{\alpha_{(i)}} + \lambda_2^{\alpha_{(i)}} + \lambda_3^{\alpha_{(i)}} - 3) - \mu_{(i)} \ln J\right] + \frac{\Lambda}{4}(J^2 - 1 - 2\ln J)$	$\mu_1 = 0.063$ N/mm^2 $\mu_2 = 0.0012$ N/mm^2 $\mu_3 = -0.01$ N/mm^2 $\alpha_{1,2,3} = 1.3, 5.0, -2.0$

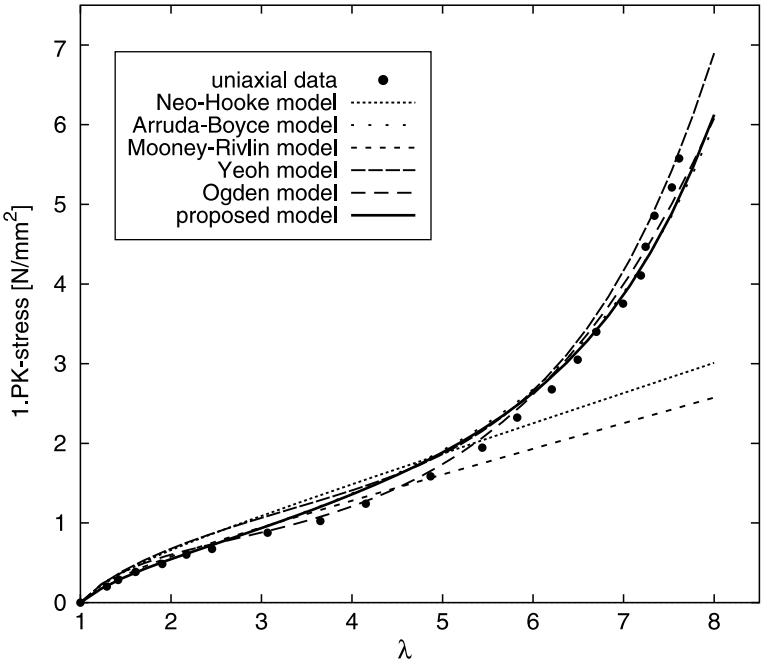

Fig. 28. Results of the uniaxial tension simulations.

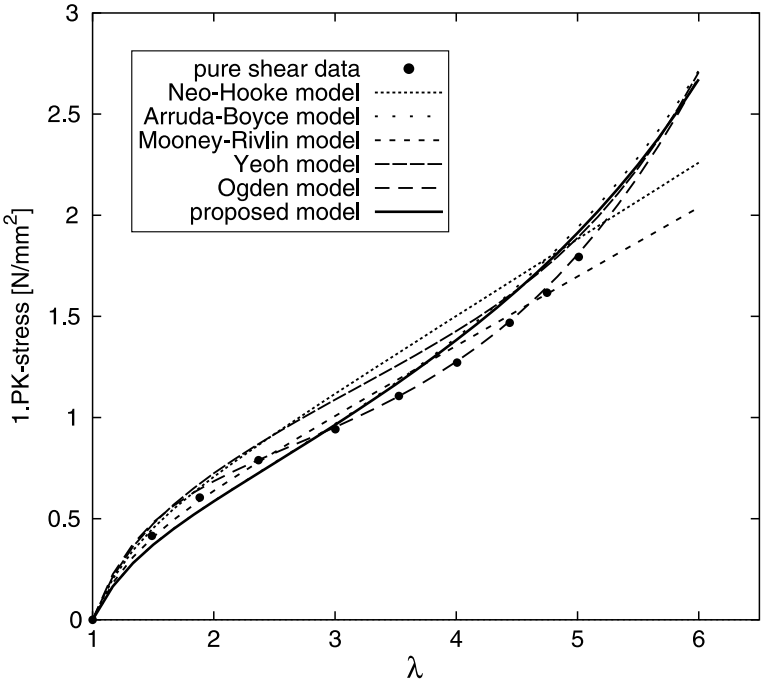

Fig. 29. Results of the pure shear simulations.

shows the S-shape behaviour, but the stress values are much too high. AB and BR yield again similar results. Both models show too soft a behaviour in the small strain regime but the overall agreement can be considered to be satisfactory. The Yeoh model is again distinguished through an extreme S-shape. In this experiment it is

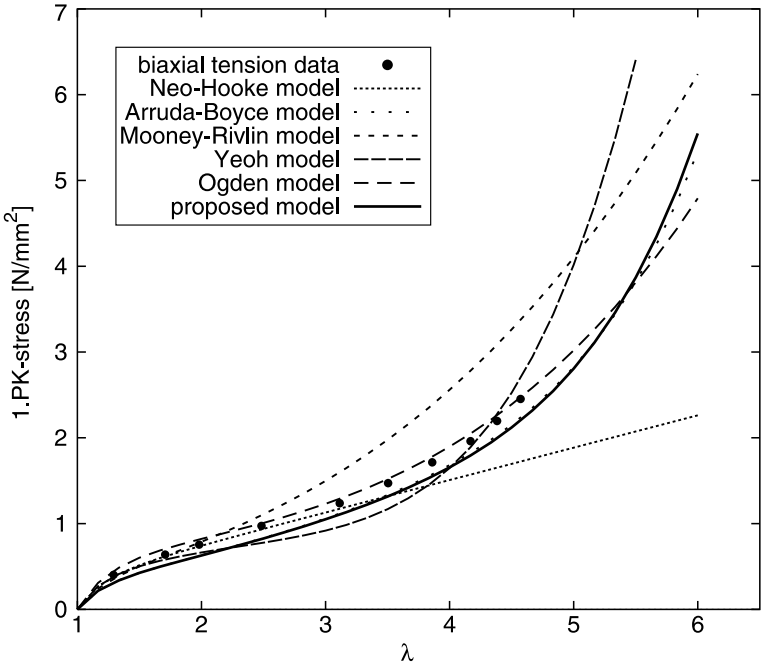

Fig. 30. Results of the biaxial tension simulations.

clearly visible that the latter model becomes too stiff in the large stretch domain. At last, as in the previous tests, the Ogden model reproduces the experimental data in an excellent manner.

In general it can be said that the AB model and the BR approach are able to reproduce the material response of the experiments in all three deformation states very well. As expected more or less the same results are obtained which is justified by the same micro mechanical approach. Both models are based on the Langevin statistics with the difference that the BR model uses more terms in the Taylor expansion of the Langevin function.

Only the Ogden model which, however, includes six material parameters is superior to the approaches AB and BR. The material parameters are not micro mechanically motivated and therefore more difficult to determine than the values of n, N, ϑ and φ.

7. Conclusions and outlook

In the present contribution we have developed a micro mechanically based finite element approach to model the finite deformation behaviour of rubber-like elastomers. The main advantage of the suggested procedure is that only physically based parameters are used. These are n (the number of chain segments), N (the number of chains per reference volume) and the parameter γ which depends on the valence and the rotation angle of the chains. The only user-defined parameter is f_{chain}, the ratio of the number of chains per reference volume with respect to the number of truss element per reference volume.

The comparison with experimental results shows that the present approach serves to model the material behaviour of rubber-like in different deformation states very well. We obtain results of the quality of the Arruda–Boyce model which is easily explained by the fact that both concepts have the same micro mechanical basis.

The proposed approach can be additionally used to simulate the deformation of networks with complex shape and arbitrary chain configurations. It is further possible to study the interaction between the micro and the macro mechanical behaviour in detail. In particular, we have investigated the influence of the chain length on the macroscopic response as well as the effects of non-affine deformation and inhomogeneous chain bundle arrangements.

Concerning the practical use it is important to state that the numerical effort of the new concept is comparable to the computational cost of conventional finite element simulations of rubber-like structures. This is confirmed by means of several studies of convergence which show that convergence of the solution with respect to the number of elements is achieved by means of rather coarse meshes.

Future work should be directed to simulate inelastic material behaviour, e.g. the Mullins' effect and viscoelasticity. Inelasticity at the macro level can be explained at the micro level by the effects of chain breakage and reconnection. The present model offers the possibility to replace the constant parameter f_{chain} by a deformation-dependent function. In this way the variation of the number of chains in dependence of stress or deformation can be modelled without noticeable additional effort. A further extension of the concept should concern the modelling of filled polymers which are of major importance in industrial applications. One promising idea to include fillers into the polymer network model is to replace certain clusters of tetrahedrons as filler particles.

References

Anand, L., 1996. A constitutive model for compressible elastic solids. Computational Mechanics 18, 339–355.

André, M., Wriggers, P., Bertram, C., 2001. Simulation of effective rubber properties during cross-linking using simple network model. In: Besdo, D., Schuster, R.H., Ihlemann, J. (Eds.), Constitutive Models for Rubber II, pp. 223–228.

Arruda, E.M., Boyce, M.C., 1993. A three-dimensional constitutive model for the large stretch behavior of rubber elastic materials. Journal of the Mechanics and Physics of Solids 41 (2), 389–412.

Ball, R.C., Doi, M., Edwards, S.F., Warner, M., 1981. Elasticity of entangles networks. Polymer (22), 1010–1018.

Besdo, D., Ihlemann, J., 2003. Properties of rubberlike materials under large deformations explained by self-organizing linkage patterns. International Journal of Plasticity 19, 1001–1018.

Bischoff, J.E., Arruda, E.A., Grosh, K., 2002. A microstructurally based orthotropic hyperelastic constitutive law. Journal of Applied Mechanics 69, 570–579.

Chiumenti, M., Valverde, Q., Ageletde Saracibar, C., Cervera, M., 2002. A stabilized formulation for incompressible elasticity using linear displacement and pressure interpolytions. Computer Methods in Applied Mechanics and Engineering 191, 5253–5264.

Flory, P.J., 1969. Statistical Mechanics of Chain Molecules. Interscience Publishers.

Flory, P.J., Rehner, J., 1943. Statistical mechanics of cross-linked polymer networks. Journal of Chemical Physics 11, 512–520.

Gao, J., Weiner, J.H., 1991. Chain force concept in systems of interacting chains. Macromolecules 24, 5179–5191.

Gaylord, R.J., 1979. Entanglement and excluded volume effects in rubber elasticity. Polymer Engineering and Science 19, 263–266.

Hölzl, T., Trautenberg, H.L., Göritz, D., 1997. Monte carlo simulations on polymer network deformation. Physical Review Letters 79 (12), 2293–2296.

James, H.M., Guth, E., 1943. Theory of the elastic properties of rubber. Journal of Chemical Physics 11, 455–481.

Kuhn, W., 1936. Beziehung zwischen Molekülgrösse, statistischer Molekülgestalt und elastischen Eigenschaften hochpolymerer Stoffe. Kolloid-Zeitschrift 76, 258–271.

Kuhn, W., Grün, F., 1942. Beziehung zwischen elastischen Konstanten und Dehnungsdoppelberechnung hochelastischer Stoffe. Kolloid-Zeitschrift 101, 248–271.

Lang, M., Göritz, D., Kreitmeier, S., 2003. The effect of spatially inhomogeneous mixing of polymer and cross-links for end-linked polymer networks. In: Busfield, J.J.C., Muhr, A.H. (Eds.), Constitutive Models for Rubber III, pp. 195–202.

Lodge, A.S., 1999. An Introduction to Elastomer Molecular Network Theory. The Bannatek Press, Madison.

Lulei, F., Miehe, C., 2001. A physically-based constitutive model for finite viscoelastic deformations in rubber polymer based on a directly evaluated micro–macro-transition. In: Besdo, D., Schuster, R.H., Ihlemann, J. (Eds.), Constitutive Models for Rubber II, pp. 117–125.

Mooney, M., 1940. A theory of large elastic deformation. Journal of Applied Physics 11, 582–592.

Ogden, R.W., 1972. Large deformation isotropic elasticity-on the correlation of theory and experiment for incompressible rubberlike solids. Proceedings of the Royal Society of London A 326, 565–584.

Rivlin, R.S., 1948. Large elastic deformations of isotropic materials, I, II, III. Philosophical Transactions of the Royal Society of London 240 (A), 459–525.

Treloar, L.R.G., 1943. The elasticity of a network of long-chain molecules I/II. Transactions of the Faraday Society 39, 36–41, 241–246.

Treloar, L.R.G., 1944. Stress–strain data for vulcanized rubber under various types of deformation. Transactions of the Faraday Society 40, 59–70.

Wall, F.T., 1942. Statistical thermodynamics of rubber. II. Journal of Chemical Physics 10, 485–488.

Wittkop, M., Sommer, J.U., Kreitmeier, S., Göritz, D., 1994. Monte carlo simulations of a single polymer chain under an external force in two and three dimensions. Physical Review E 49 (6), 5472–5476.

Wriggers, P., 2001. Nichtlineare Finite-Element-Methoden. Springer-Verlag.

Wu, P.D., van der Giessen, E., 1993. On improved network models for rubber elasticity and their applications to orientation hardening in glassy polymers. Journal of the Mechanics and Physics of Solids 41, 427–456.

Yeoh, O.H., 1993. Some forms of the strain energy function for rubber. Rubber Chemistry and Technology 66 (5), 754–771.

Zienkiewicz, Taylor, R.L., 2000. The Finite Element Method. The Basis, vol. I. Butterworth-Heinemann.